Available online at www.sciencedirect.com
ScienceDirect
Applied Catalysis A: General 322 (2007) 76–91
APPLIED CATALYSIS A: GENERAL
www.elsevier.com/locate/apcata

Understanding and predicting improved sulfide catalysts: Insights from *first principles* modeling

P. Raybaud *

Institut Français du Pétrole, Direction Chimie et Physico-Chimie Appliquées, 1 & 4 Avenue de Bois-Préau, 92852 Rueil-Malmaison Cedex, France

Available online 4 January 2007

Abstract

This paper is a review of recent advances accomplished in the field of hydrotreatment (HDT) sulfide catalysts and using theoretical approaches based on the density functional theory (DFT) combined with thermodynamic models and microkinetic models. We illustrate first numerous concepts of modern DFT simulation for a better understanding of the industrial Co(Ni)MoS active phases: localization and role of the promoter, electronic properties and morphological changes induced by the reaction conditions or by promoter addition. Then, it is shown how support effects can be modeled by DFT to provide new insights on the local structure and energy stability of the active phase-support interface, where characterization techniques reach their limits. The comparison between γ-alumina and anatase-TiO_2 supports is chosen as a relevant example. Finally, DFT simulations and microkinetic models help to rationalize ''volcano-curve'' type relationships between hydrodesulfurization (HDS) or hydrogenation (HYD) activities and the calculated sulfur–metal bond energy descriptor. This approach opens new routes to use systematic DFT simulations as a predictive tool. Perspectives for DFT simulations in the area of catalysis by sulfides are suggested.

Keywords: Density functional theory (DFT); Hydrodesulfurization (HDS); Hydrotreatment (HDT); Transition metal sulfides; MoS_2; CoMoS; NiMoS; Supports; γ-Alumina; Anatase-TiO_2; Volcano curves

1. Introduction

Due to severe environmental constraints, the production of ever cleaner fuels by hydrotreating processes remains a major concern of the refining industry. The challenges for catalyst suppliers are to provide increased hydrodesulfurization (HDS) activity catalysts meeting specific targets for the ultra low sulfur diesel markets (less than 10 ppm sulfur by 2009) while ever heavier petroleum feeds are to be treated [1,2]. Given the complex nano-scale structure of HDS catalysts made of γ-alumina supported Co(Ni)MoS sulfide, their continuous improvement requires the capability to take up multiple research issues raised by the properties of the Co(Ni)MoS active phase, the support γ-alumina phase, and the two interacting phases in reaction conditions. Indeed, improvements of the active phase are rarely obtained without a careful consideration of its interaction with the support either at the preparation step or during reaction.

In the ''scientific history'' of HDT catalysis by transition metal sulfides (TMS), numerous cutting-edge experimental techniques were used to better characterize the catalytically active phases [3,4]. A wide range of experimental evidence was thus available before any relevant theoretical data were available. The non-exhaustive list of experimental techniques involved in this tremendous characterization task consists of transition electron microscopy (TEM) [5,6], X-ray photoelectron spectroscopy (XPS) [7–10], Mössbauer spectroscopy [11], laser Raman spectroscopy [6,12], extended X-ray absorption fine structure (EXAFS) [13–17], and IR spectroscopy [18,19]. These techniques furnished the detailed features of the so-called Co(Ni)MoS active phase made of MoS_2 layers with a stacking close to 1 [20] and nanometer sizes (less than 30 Å), ''decorated'' by Co or Ni at the edges. However, for a better understanding and new improvements, a even more precise atomistic description of the Co(Ni)MoS phase was required, while different inconsistent atomistic models for the promoter location were proposed. It was thus a challenge for the

* Tel.: +33 1 47 52 71 84; fax: +33 1 47 52 70 58.
E-mail address: pascal.raybaud@ifp.fr.

0926-860X/$ – see front matter © 2007 Elsevier B.V. All rights reserved.
doi:10.1016/j.apcata.2007.01.005

emerging technique based on *first principles* modeling to bring expected insights and concepts contributing to new progresses in this area.

Regarding the support effects on the active phase, two aspects must be considered. On the one hand, a very abundant experimental research (probably as abundant as for TMS) was carried out on the γ-alumina support since the pioneering work of Lippens and de Boer [21] using techniques such as nuclear magnetic resonance (NMR) [22–24], vibrational spectroscopies [25–28], XRD [29] and TEM [30]. However, the rational description of the γ-Al_2O_3 bulk structure and the surface species (hydroxyls, acid–base sites, etc.) suffered from ambiguous interpretation due to a lack of atomistic investigation. On the other hand, the impact of the support on the Co(Ni)MoS active phase properties was investigated by many research groups. Two reviews by Breysse et al. [31,32] illustrate in detail experimental results in this field. The intrinsic HDS activity (expressed per Mo site) was found to be about 4.4 times higher for titania supported MoS_2 catalysts compared to γ-alumina [33]. However, the expected synergy effect when adding the promoter is significantly weaker on titania compared to γ-alumina. Numerous proposals were put forward to explain these observations such as electronic effects [33], orientation effects [34] or indirect promotion by Ti [35–37]. This underlines that there was a clear need for a better understanding the nature of interaction between the support and the active phase. Even if EXAFS data provided some insights on the local distances and coordination at the interface between the active phase and the support [38], it remained very difficult to extract an atomistic representation of the active phase–support interface. As a consequence, a double answer was expected from modern *first principles* techniques in this area: to furnish improved models for support's surfaces (γ-alumina) and to address the subtle effects of active phase–support interaction.

Thanks to the giant step forward provided by the development of density functional theory (DFT) [39,40] and its elegant implementation in efficient softwares such as VASP [41,42], DACAPO [43], Wien2k [44], CASTEP [45,46], $DMol^3$ [46,47], modern *first principles* modeling provide a rational way to investigate the active sites present at the catalytic surface. The most recent DFT simulations of γ-alumina supported MoS_2 catalyst show that the gap between theoretical approaches and the real world is considerably reduced [48]. Combining DFT calculated energy values with thermodynamic models or microkinetic models enables to include the effects of partial pressures of H_2S or H_2 as found in HDS reactions and to explore periodic trends.

The goal of the present paper is thus to provide an overview of relevant achievements obtained through *density functional* modeling of HDS catalysts. After a first section devoted to a brief presentation of some methodological aspects, we focus on the MoS_2 and Co(Ni)MoS active phases where various key scientific questions about the promoter location, morphology and effects of reaction conditions are addressed in combination with experiments. In Section 3.2, we illustrate the most recent advances provided by DFT modeling and show the way to investigate aspects as subtle as the nature of the sulfide–support interaction. In particular, we focus on the comparison between two important oxide supports used in HDS: γ-alumina and anatase-TiO_2. The challenge for DFT is raised by the size limit of the tractable simulation supercells and care is needed to represent as rigorously as possible supported active phases by robust models.

Finally, we address probably one of the most exciting challenge: the rational design of sulfide catalysts. Based on structure–activity relationships, we outline how DFT modeling may open exploratory routes for the pre-screening of new potential active phases. Combining DFT calculated chemical descriptors with microkinetic modeling enabled volcano curves to be built correlating HDS or HYD turnover frequencies and relevant DFT descriptors. This aspect represents a growing interest within the context of the emerging high throughput experimentations in catalysis.

2. Methods

The general approach which combines DFT calculations and the chemical potential of the gas phase was previously undertaken to study surface thermochemistry of GaAs [49], c-BN [50] and α-Fe_2O_3 [51]. To our knowledge, this approach successfully applied to MoS_2 and Co(Ni)MoS systems was firstly reported in [52,53]. More recent studies have also used this systematic approach to include the effect of adsorbed hydrogen on the sulfide surfaces [54,55]. This is an elegant way to bridge the gap between DFT calculations (carried out at 0 K) and realistic reaction conditions.

To determine by theoretical approaches the stable chemical species on the catalytic surface in reaction conditions (p_i, T) at thermodynamic equilibrium, one must minimize the surface energy given by the following general expression:

$$\Gamma_{hkl}(p_i, T, \theta^i_{hkl}) = \Gamma^0_{hkl} + \sum_i \theta^i_{hkl}(E^i_{\text{ads}} + \Delta\mu_i) \quad (1)$$

$$\Delta\mu_i(T, p_i) = h^0_i - Ts^0_i + RT\ln\left(\frac{p_i}{p^0}\right) - e_i \quad (2)$$

$\Gamma_{h\,k\,l}$ is the surface energy of the surface with ($h\,k\,l$) crystallographic orientation (for instance one of the edges of the Co(Ni)MoS nano-crystallites). Γ^0_{hkl} is the surface energy of the reference ($h\,k\,l$) surface (generally in vacuum or in absence of any adsorbed species). E^i_{ads} is the adsorption energy of the molecule i, such as H_2S, H_2O or H_2 in the cases investigated so far. The most stable adsorption mode of the molecule i (either dissociative or non-dissociative) is determined as a function of its surface coverage θ^i_{hkl}. The molecule may thus generate different types of species (M–H_2S, M–H_2, M–H_2O, M–SH, M–OH, MH, etc.) depending on its stable adsorption mode defined by the most exothermic adsorption energy.

$\Delta\mu_i$ is the chemical potential of the molecule i in the gas phase: it depends on the partial pressures (p_i) of H_2S, H_2O or H_2 and temperature (T) according to (2). Fig. 1 gives the values of $\Delta\mu_s$ as a function of p_{H_2S}, p_{H_2} and T ranges considered in this manuscript as explained elsewhere [48,52].

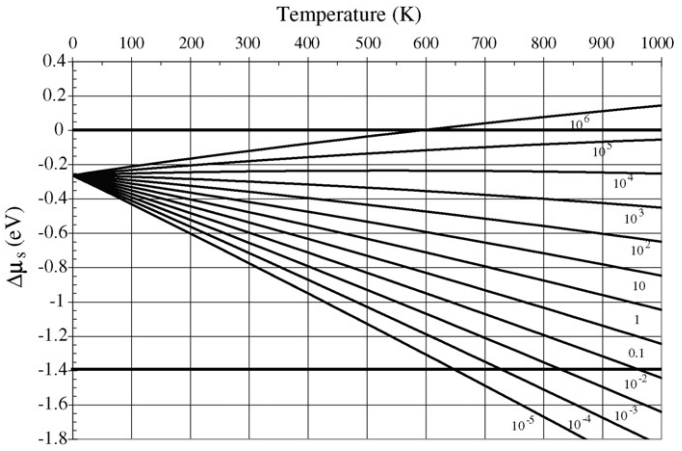

Fig. 1. $\Delta\mu_s$ values as a function of temperature and p_{H_2S}/p_{H_2} ratio, i.e. $\Delta\mu_S = h_{H_2S}(T) - h_{H_2}(T) - E_{S_\alpha} - T\lfloor s_{H_2S}(T) - s_{H_2}(T)\rfloor + RT\ln(p_{H_2S}/p_{H_2})$ as explained in previous works (from Ref. [48]).

Eqs. (1) and (2) furnish a direct connection between the chemical state of the catalytic surface and reaction conditions assuming that at equilibrium the stable state of the surface is defined as the one minimizing its surface energy. At this stage, no assumption is made on the methodology used to calculate the energy terms in (1) and (2). When considering chemical processes involving bond breaking and bond formation at a surface, the so-called *ab initio* methods (excluding any empirical fits) are required. The formalism of the density functional theory (DFT) enables the Schrödinger equations to be solved for complex systems with a minimal set of approximations [39,40]. From a practical point of view, the software implementation of the so-called *first principles* modeling technique furnishes the best compromise between computational resources and system sizes required for realistic simulation.

In the present case, the energy values such as Γ^0_{hkl}, E^i_{ads} and $\Delta\mu_i$ are the outcome of simulations based on DFT within the generalized gradient approximation (GGA) [56]. To solve the Kohn–Sham equations, numerous works reported herein use the Vienna *Ab initio* Simulation Package (VASP) [41,42], other cited works are based on a very similar methodology (such as the DACAPO software [43]). The ion-electron interactions are treated by pseudopotentials such as Vanderbilt ultrasoft pseudopotentials [57,58] for earlier works reported in this paper, and within the projected augmented wave (PAW) formalism [59] for more recent results. For simulations of solid phases with delocalized electronic charges it is efficient to employ a plane wave basis set to project the wavefunctions in a 3D-supercell representing the systems (bulk or slabs) with periodic boundary conditions. Other DFT works on sulfides reported in this review may also use atomic basis sets [47] (such as provided by the DMol^3 methodology [46]) either in a 3D-supercell or on a finite size clusters. All detailed hypothesis of calculations (such as electronic convergence criteria, energy cut-off, *k*-point mesh, etc.) can be found in papers cited herein.

DFT calculations enable the geometry optimization of all structures, which is crucial for determining correct energetics and structure of the surfaces. It is known that surface relaxation contributes significantly to the resulting energy. As a consequence, local interatomic distances are expected with a precision of ±0.05 Å comparable with the EXAFS technique. In particular, DFT techniques proved to be efficient in describing the bulk properties of numerous transition metal sulfides [60–63], and to furnish derived properties such as vibrational frequencies to be compared with IR spectroscopy (for hydroxyl groups, CO molecule, etc.).

For kinetic investigations, the saddle points' search on the potential energy surfaces by means of efficient approaches such as the "Nudged Elastic Band (NEB)" method [64] is often used to determine transition states and activation energies of the elementary steps of reactions (H_2 activation, S–C bond breaking, S-removal, etc.). Numerous examples use this technique to investigate complex mechanisms taking place in various catalytic systems such as zeolites [65] or metals [66]. In what follows, we will report results recently obtained in of the reactivity of sulfides thanks to this methodology.

3. Results and discussion

3.1. Co(Ni)MoS active phase

3.1.1. Non-promoted MoS_2

3.1.1.1. Characterization of sites and morphological effects. As mentioned in introduction, various experimental techniques established that the active phase of industrial HDT catalysts consists of MoS_2 nano-layers promoted by Co or

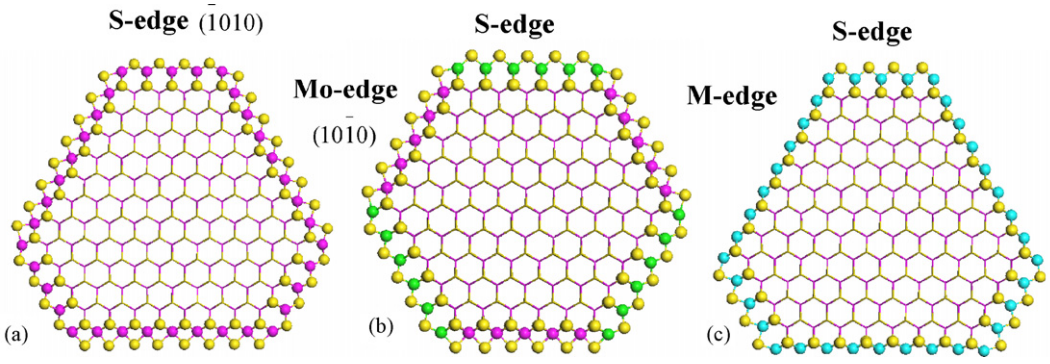

Fig. 2. DFT calculated equilibrium morphologies in HDS conditions of the (a) non-promoted MoS_2 active phase, (b) CoMoS with Co at the S-edge only, and (c) NiMoS with Ni at the S-edge and Mo-edge (extracted from Refs. [85,72]). Only one Mo-edge has been substituted by Ni Yellow balls: sulfur; magenta balls: molybdenum; green balls: cobalt; blue balls: nickel. (For interpretation of the references to colour in this figure legend, the reader is referred to the web version of the article.)

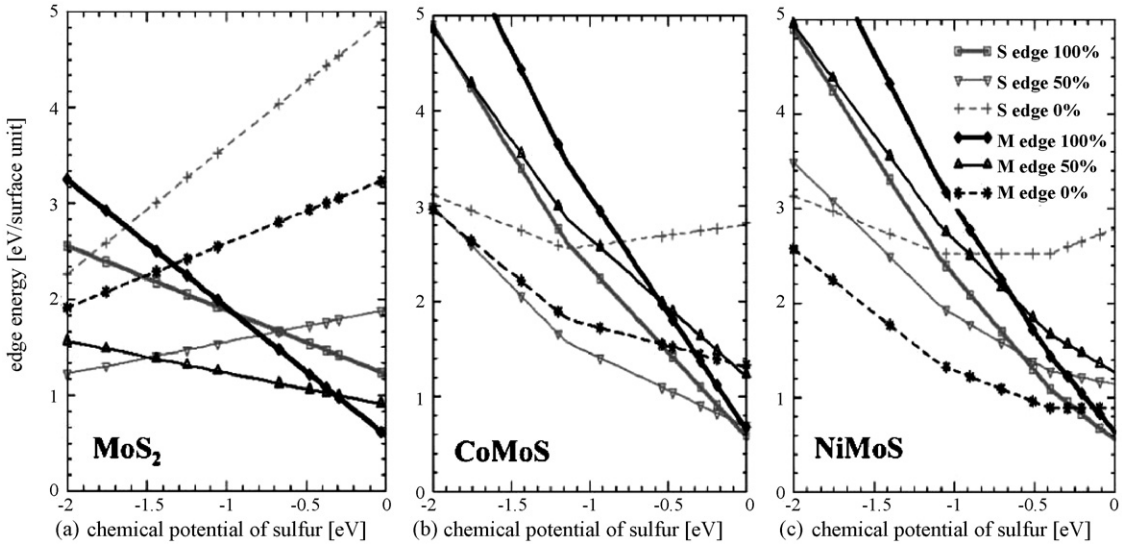

Fig. 3. Variation of the edge energy as a function of the chemical potential of sulfur for the non-promoted and Co(Ni)MoS active phases (from Ref. [85]). HDS conditions are close to $\Delta\mu_s = -0.9$ eV.

Ni edge decoration. However, the non-promoted MoS_2 has also been the subject of numerous studies for purpose of comparison with the promoted systems. Under HDT conditions, the MoS_2 phase exhibits two competing active edges: the $(1\,0\,\bar{1}\,0)$ molybdenum edge and the $(\bar{1}\,0\,1\,0)$ sulfur edge, while the (0 0 1) basal plane remains inactive (Fig. 2).

DFT simulations reveal the electronic and structural properties of these two edges [67]. The electronic features of the coordinatively unsaturated Mo-edge sites (also called "CUS") are put forward by the analysis of the projected density of states close to the Fermi energy. The unsaturated surface sites exhibit a closing of the bulk semiconducting gap. Occupied *d*-states at the Fermi energy level are responsible of the metallic character of the Mo-site [67,68] and are at the origin of the back-donation into the $2\pi^*$ antibonding orbital of CO [69]. Unoccupied *d*-states just above the Fermi level, are clearly responsible for the strong adsorption energies of electron donating species such as sulfur atoms [52,70] and thiophene molecules [71] at the Mo-edge, where unsaturated Mo-sites act as Lewis sites.

To investigate the sulfur adsorption and desorption process on the two edges of the non-promoted phase in typical sulfo-reductive conditions, the use of a thermodynamic model as presented in Section 2 is required. This approach enables the determination of the local structures of both edges as a function of the chemical potential of sulfur (depending on temperature and partial pressures of H_2S and H_2) [52,72]. Fig. 3(a) shows that in typical HDS conditions ($T = 673$ K and $p_{H_2S}/p_{H_2} = 0.05$, i.e. close to a chemical potential of -0.9 eV according to Fig. 1), the edge energies are minimal when the Mo- and S-edge are 50% sulfur covered (the bulk structure with 100% sulfur is taken as

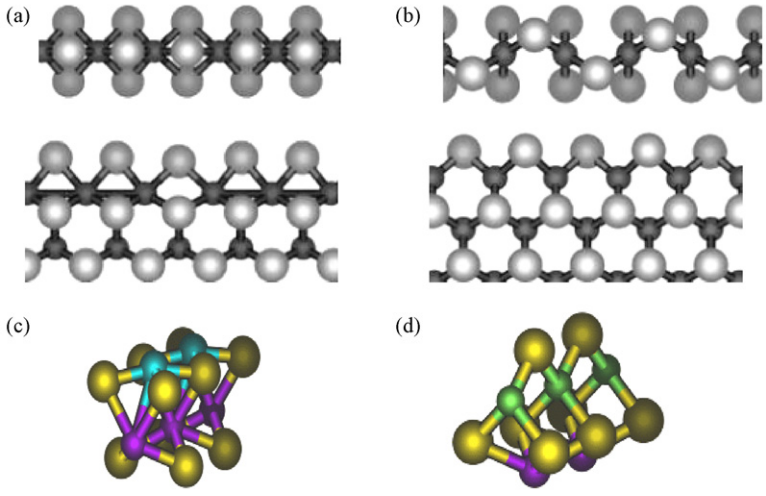

Fig. 4. Local structure of the edges in HDS conditions ($\Delta\mu_s = -0.9$ eV in Figs. 1 and 3): (a) top and side view of the Mo-edge, (b) S-edge (grey balls: sulfur; black balls: molybdenum), and (c) 3D-view of the Mo-edge promoted by Ni, (d) S-edge promoted by Co (yellow balls: sulfur, magenta balls; molybdenum, blue balls: nickel, green balls: cobalt) (from Refs. [72,85]). (For interpretation of the references to colour in this figure legend, the reader is referred to the web version of the article.)

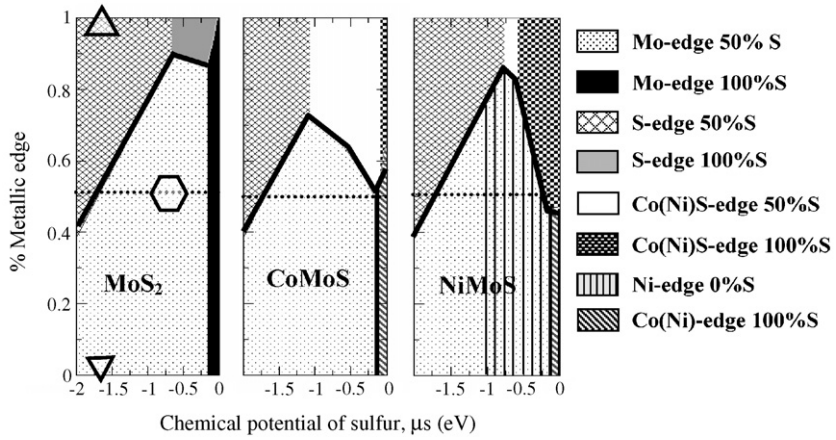

Fig. 5. Equilibrium morphologies (thick lines) and edge compositions of the nano-crystallites as a function of $\Delta\mu_s$. The ordinate represents the percentage of $(1\,0\,\bar{1}\,0)$ metallic edge exposed for the corresponding equilibrium morphology (from Ref. [85]).

reference). The corresponding local structures are given in Fig. 4(a) and (b) showing that the Mo-atoms of the Mo-edge are six-fold coordinated, while at the S-edge the Mo-atoms are four-fold coordinated.

The calculation of the edge energies by Eq. (2) makes it possible to deduce from Gibbs–Curie–Wulff laws the equilibrium morphology of the MoS_2 nano-crystallites. As depicted in Fig. 5(a), the percentage of the Mo-edge is expressed as a function of the chemical potential of sulfur. Depending on the reaction conditions, not only the sulfur coverage at the edge of the nano-crystallite changes but also the shape of each individual MoS_2 nano-layer. According to these DFT calculations, the predicted shape is close to a triangle for values of chemical potential of sulfur close to 0 (corresponding to high partial pressure of H_2S according to Fig. 1) and S-dimers are present at the edges. For reductive environment such as in HDS conditions, the shape is close to a deformed hexagon (Fig. 2) exhibiting slightly more Mo-edge than S-edge (with S-bridging atoms at the edges). The morphology change of the MoS_2 nano-sheets is confirmed by scanning tunnel microscopy (STM) experiments revealing either a triangular shape [73] or a hexagonal one depending on the sulfiding conditions of gold supported MoS_2 clusters [74].

3.1.1.2. Reactivity. The thermodynamical approach including the chemical potential of the gas phase is again required to explore stability of hydrogen at the edges [54,55,75] and the formation of Mo–SH and M–H species at the edges as a

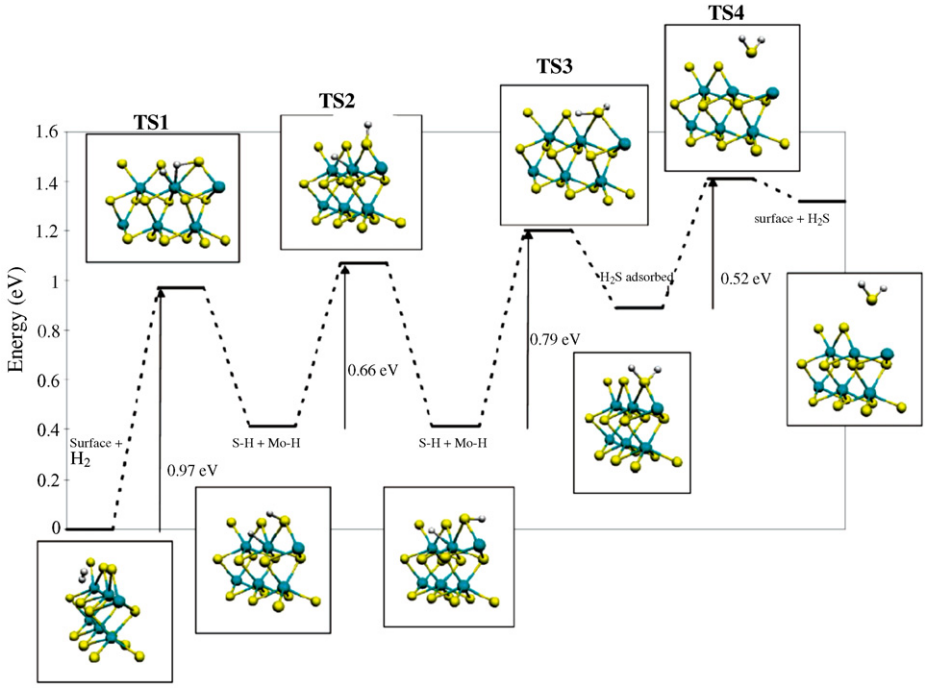

Fig. 6. Reaction pathway for the first S-vacancy creation on the Mo-edge covered by 50% S. All intermediates and transition states are represented. Yellow balls: sulfur; blue balls: molybdenum, white balls: hydrogen (from Ref. [76]). (For interpretation of the references to colour in this figure legend, the reader is referred to the web version of the article.)

function of the temperature and partial pressures of H_2S and H_2 [54,75]. Atomic hydrogen can be stabilized at the edges for conditions beyond HDS conditions (i.e. very high pressure or very low temperature) meaning that Mo–SH and M–H are metastable species on non-promoted systems. Paul and Payen investigated further the mechanism of H_2 activation and sulfur vacancy formation [76] in order to identify the kinetic limiting steps. Fig. 6 depicts one relevant example of transition states determination using the NEB method (see Section 2): for the full reaction pathway of the first sulfur vacancy creation on the Mo-edge four transition states are found. This detailed analysis shows that the creation of one sulfur vacancy is kinetically more favorable on the Mo-edge (with 50% sulfur coverage) than on the S-edge (with the same S-coverage). Furthermore, for such S-content at the Mo-edge (stable in HDS conditions), the hydrogen dissociation is the limiting step with an activation barrier for TS1 of about 1.0 eV. Similar activation energies have been also reported by other studies [77,78].

The DFT determination of HDS reaction pathways of thiophene [79], benzothiophene (BT), 4-methylbenzothiophene (MBT) [80] on MoS_2 edges reveals that energy profile of the reactions depends on the adsorption mode, which is function of the S-coverage at the edges (i.e. number of S-vacancy). The η_5 adsorption mode (π bonding mode) of thiophene strongly distorts and activates the molecule towards hydrogenation and S–C bond breaking resulting from a donation/back-donation process involving the occupied and unoccupied Mo *d*-states close to the Fermi energy (see previous section). The η_1 adsorption involving mainly the donation from the S lone pair into the acceptor Mo *d*-states induces a weaker activation of the thiophene. The HDS pathway exhibits unfavorable steps as first and third mono-hydrogenation. To a certain extent, the energy profile in the η_1 mode remains closer to the gas phase profile. This study shows that the regeneration of the coordinatively unsaturated site (CUS) is the most endothermic step. Similar results are obtained for the HDS energy profiles of the adsorption of BT and 4-MBT by Cristol et al. [80]. For 4,6-dimethyldibenzothophene (4,6-DMDBT) the S-edge would be the favorable adsorption edge in η_1 configuration leading preferentially to the direct desulfurization route [81]. Stacking faults in the MoS_2 layers may offer new adsorption modes for DMDBT by diminishing the steric hindrances [81]. According to these authors, the formation of CUS is a required step for the HDS reaction on non-promoted system.

The Schweiger et al.'s study points out that size effects and corner effects of the MoS_2 nano-crystallites can stabilize S-deficient states [72]. By increasing the size of the MoS_2 cluster, the creation of one S-vacancy at the Mo-edge (i.e. one single CUS) initially covered by 50% sulfur (as depicted in Fig. 4(a)) becomes favorable for cluster sizes with an edge length greater than nine Mo atoms (i.e. for particle's diameters greater than 30 Å). This would justify the aforementioned pathway for HDS. In some STM experiments with specific conditions, it has been observed the formation of S-vacancy [73] and thiophene adsorption on CUS [82]. Furthermore, DFT calculations have also shown that the creation of one S-vacancy at the crystallite's corner is even more favorable [72]. These results concerning the stability of very low concentration CUS and HDS reaction pathways on CUS remain fully valid as one possible chemical route for HDS on non-promoted catalyst.

Other STM experiments reveal that the thiophene transformation into butenethiol may occur on the metallic rim of the basal plane close to the edge [82,83], in absence of CUS. This rather unexpected chemical route is observed for the specific STM experimental conditions where atomic hydrogen is supplied in the UHV chamber. This source of atomic hydrogen could enhance the reactivity of the MoS_2 clusters by generating adsorbed hydrogen on sulfur dimers not stable in HDS conditions according to DFT studies [52,55,75]. Even if this second chemical route cannot be overlooked, the extrapolation to real HDS conditions remains difficult. Furthermore, to obtain the fully desulfurized product after the butenethiol formation, the existence of CUS is required at least for the second S–C bond breaking: for that, scenario as previously described [79–81] remain relevant.

As a consequence, it seems that two chemical routes involving two types of sites for HDS reaction may take place on non-promoted systems. The first one involves the formation of CUS even at low edge concentration according to [72]. The second route, recently invoked in [83], would not need the presence of CUS for the first hydrogenation of thiophene. However, this brim sites' route, limited by the hydrogen dissociation step [76,77], is not sufficient to explain the complete HDS pathway of sulfur compounds by itself: the existence of CUS remains again mandatory. In both cases, the catalytic activity of the non-promoted system remains weak mainly due to the high S–Mo bond energy at the edges, implying a poisoning effect by S-species, preventing adsorption of reactants or H_2 dissociation. This limitation of MoS_2 systems can be overcome by the promoters' addition as explained in the next section.

3.1.2. Co(Ni)MoS

3.1.2.1. Characterization of sites and morphological effects. As mentioned in introduction, many experimental techniques (EXAFS, Mössbauer spectroscopy, XPS) were used to characterize the Co(Ni)MoS ternary phase. While Mössbauer spectroscopy [11] and XPS [7–10] revealed the specific signature of Co atoms engaged in the new CoMoS phase, EXAFS gave relevant insights into the local environment of the promoter atoms (Co or Ni) in the structure: Co(Ni)–Mo distances of 2.75–2.90 Å and Co(Ni)–S distances of 2.10–2.20 Å [13–15]. However, some ambiguities remained because different atomistic models (including the old pseudo-intercalation model [84]) were compatible with the experimental data. DFT simulations were thus mandatory to discriminate between the proposed atomistic models on the basis of total energy calculations. Raybaud et al. investigate seven possible locations for Co in the structure: intercalation, pseudo-intercalation (either in octahedral or tetrahedral position), bulk substitution, edge substitution, and edge addition [53], including the effect of sulfur coverage at the edge. They demonstrated that the most stable models are those where Co (or Ni) substitutes Mo at the S- or Mo-edge (Fig. 4(c) and (d)).

The optimized local Co–Mo and Co–S distances for these two most stable configurations are fully compatible with EXAFS analysis. Schweiger et al. put forward two distinct behaviors at the metallic- and sulfur-edge with respect to the promoter [85]. As shown in Fig. 3(b) and (c), they found that Co is more stable in substitution at the S-edge than at the Mo-edge due to a smaller edge energy at the S-edge. This preferential location of Co is also supported by other DFT simulations [70] and STM experiments on gold supported CoMoS [86]. The presence of the Co (or Ni) promoter (acting as a surfactant) implies that the morphology is modified as depicted in Figs. 2(b) and (c) and 5(b) and (c). For HDS conditions, the CoMoS nano-crystallites are closer to a hexagonal shape than in the case with non-promoted particles. It is interesting to notice that the DFT calculated morphology remains compatible with the geometrical model earlier proposed by Kasztelan et al. [140].

As a consequence, the sulfo-reductive conditions (partial pressure of H_2S/H_2 and temperature) appear as a key parameter for controlling the morphology of the active phase and thus the type of exposed active sites. However, one cannot overlook other effects during the complex preparation and synthesis steps. On the one hand, kinetic limitations might take place during the precursors' impregnation, genesis of the active phase (including sulfidation and activation), on the other hand, interaction with the support or with any added chemical species (counter ions, chelating agents) during the synthesis pathways may modify the equilibrium morphology: the latter acting as surfactants and surface energy modifiers. Besides support's effects presented in Section 3.2, some of these aspects could represent challenging investigations for future DFT simulations.

Fig. 5(b) shows that the sulfo-reductive conditions have also an impact on the stability of the CoMoS phase. If the chemical potential of sulfur is lower than −1.2 eV (i.e. at high H_2 partial pressure or high T accessible in certain HDT conditions), the CoMoS phase may segregate into MoS_2 and metallic Co, leading to a loss of the mixed phase and catalytic deactivation. This result agrees with Breysse et al.'s observations revealing by Mössbauer spectroscopy, XPS and X-ray emission spectroscopy that CoMoS may undergo structural modification under medium to high pressures of hydrogen or at high temperature [87,88]. For high partial pressure of H_2S, the DFT results show that the promoter is stabilized on both edges. This result implies that controlling the sulfo-reductive environment at the activation step of the catalyst may also be crucial to modify the promoter content at the edges.

Finally, the striking finding obtained for NiMoS nano-crystallites by Schweiger et al. [85] is that Ni exhibits a higher affinity for the Mo-edge than for the S-edge (Figs. 4(c) and 5(c)). For the first time, a subtle but relevant difference in the local structure is thus revealed between CoMoS and NiMoS. This result confirmed by other DFT calculations [89] may provide a new insight for the interpretation of subtle different catalytic behaviors observed between the CoMoS and NiMoS phases [90,91]. Recent characterization by infra-red of CO adsorbed on MoS_2 and Co(Ni)MoS combined with DFT calculations of the stretching wavenumber of CO provide an instructive assignment of edge sites [69,92]. In the case of NiMoS, the back-donation of d-states is significantly reduced with respect to MoS_2 and CoMoS, due to the lower density of occupied d-states at the Fermi level [53]. The resulting CO wavenumber is thus shifted to higher value compared to CO on CoMoS. Furthermore, this IR study and DFT assignment reveal that Mo-edge is partially decorated by Co or Ni, which confirms the possible existence of mixed Co–Mo or Ni–Mo sites as also invoked by earlier studies [53,89]. Such mixed sites may exhibit specific catalytic properties.

3.1.2.2. Catalytic activity. One first consequence for the catalytic activity is that the Mo substitution by Co (or Ni) implies a decrease of the S-coverage at both edges in HDS reaction conditions. This effect is due to a decrease of the sulfur–metal bond energy at the edge when Co or Ni are present. Again the analysis of the local electronic density of surface states reveals that the unoccupied states available on unsaturated Mo atoms of the non-promoted system, are filled by the Co(Ni) 3d electrons which reduce the intrinsic Lewis acid character of the site, by reducing its acceptor properties for electron donor such as sulfur atoms. This trend depends on the promoter content in decoration at the edge. If we consider the case of a system decorated by Cu at the edge, the sulfur metal bond energy is even lower according to [53]:

$$MoS_2 > Co_{0.33}Mo_{0.67}S > Co_{0.67}Mo_{0.33}S > Co_1Mo_0S > Ni_1Mo_0S > Cu_1Mo_0S \quad (3)$$

Here $M_xMo_{1-x}S$ stands for a mixed phase with x the M/Mo substitution ratio at the Mo-edge.

Similar trends are put forward for the thiophene adsorption on $MMo_{15}S_{32}$ clusters (M = Mo, Cr, Fe, Co, Ni, Cu, Zn) [93].

Investigations on WS_2 and Co(Ni)WS support the following extended trend for the sulfur metal bond energy at the edge [94]:

$$WS_2 > MoS_2 > CoWS > CoMoS > NiWS > NiMoS > CuMoS \quad (4)$$

As will be shown in detail Section 3.3, this trend in sulfur–metal bond energy is crucial for understanding periodic trends in HDT reactivity. While WS_2 and MoS_2 are relatively poor HDS catalysts, it is well known that Cu does not develop any promotion effect. As a consequence it seems that an intermediate sulfur-metal bond energy is required to exhibit the highest activity such as in Co(Ni)MoS or NiWS catalysts. Furthermore, since the sulfur metal bond energy depends on the promoter content at the edges, the control of the decoration at the edges is crucial for the HDS activity.

Several works study the activation of hydrogen on the previously defined Co(Ni)MoS edges [77,78,95]. The results obtained by Travert and colleagues are rather instructive. H_2–D_2 exchange experiments on MoS_2, CoMoS and NiMoS combined with DFT simulations, show that the H_2 activation energy is higher for non-promoted MoS_2, whereas the Co promoter decreases this barrier. This is explained by the Co–S bond energy weaker than the Mo–S energy. The basicity of an S

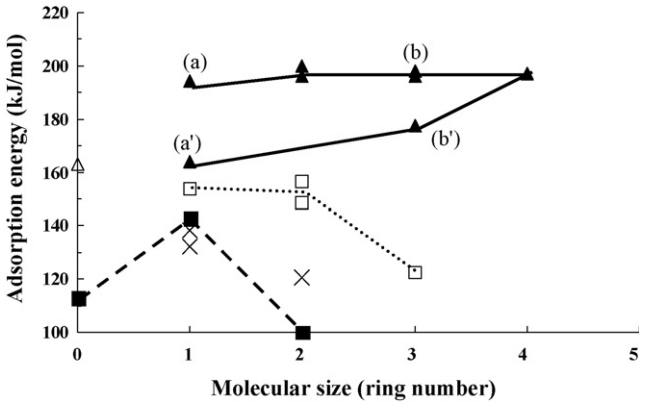

Fig. 7. Adsorption energies as a function of the molecular size (number of aromatic or heteroaromatic rings in the molecule). Azaarenes (▲)—(1) pyridine (a) and 2,6-dimethylpyridine (a′); (2) quinoleine and isoquinoleine; (3) phenantridine, benzoquinoleine (b), and acridine (b′); (4) benzophenantridine. Ammonia (△). Neutral nitrogen compounds (□)—(1) pyrrole; (2) indole and 7-methylindole; (3) carbazole. Sulfur compounds (■)—(0) H_2S; (1) thiophene; (2) DBT. Aromatics (×)—(1) benzene and toluene; (2) naphthalene.

atom linked to Co is increased, which enhances the H_2 activation. Furthermore, upon NH_3 adsorption, the S–H bond length is larger for stronger Brønsted acidic Mo–SH species than for Co–SH, which is supported by IR analysis of the pyridine adsorption on MoS_2 and CoMoS [96].

Very few DFT investigations of HDS reaction pathways on promoted systems are published so far in the literature. Todorova et al. investigated the thiol hydrogenolysis (possible intermediates in HDS reactions) and found that the promoter reduces the energy barrier for the hydrogenolysis of methanethiol CH_3SH to CH_4 by weakening the bonding of CH_3S [97]. Veilly and colleagues carried out a DFT comparison of the reaction pathways of dimethyldibenzothiophene (DBT) on MoS_2 and Co(Ni)MoS revealing that adding the promoter favors the η_1 adsorption mode of DBT involving the sulfur atom and enhancing the direct desulfurization (DDS) pathway [98,99]. However, for 4,6-dimethyldibenzothiophene (DMDBT), the steric hindrance of the methyl groups prevents DMDBT from η_1 adsorption. The promoter effect on the DDS pathway of DMDBT is thus weakened when compared to DBT, while the hydrogenation (HYD) pathway requiring flat adsorption through the benzene ring is enhanced. This result offers a new interpretation for the experimental observations on the promoter effects on the HDS of DBT and DMDBT [100].

3.1.2.3. Inhibiting effects by organonitrogen compounds. - When considering heavy crude oils to be treated nowadays and in the near future, it is crucial to compare the behaviors of organonitrogen with organosulfur compounds. In this area, one interest of applying DFT techniques is to calculate systematically adsorption energies of azaarenes, or basic nitrogen pyridine derivatives, and neutral compound such as pyrrole derivatives on NiMoS catalysts. Fig. 7 shows results obtained at IFP using the VASP methodology for calculating adsorption energies. According to Fig. 7, azaarenes compounds (such as benzophenantridine) exhibit the strongest adsorption energies ($E_{ads} = -197$ kJ/mol). For the configuration reported in Fig. 8(a), it is important to notice that benzophenantridine and other azaareenes are adsorbed in η_1 mode involving the N-atom on the Mo site of the NiMoS catalyst. This explains why some methyl substituted compounds (such as 2,6-dimethylpyridine) exhibit reduced adsorption energies. In contrast, all neutral nitrogen compounds such as carbazole represented in Fig. 8(b) are less strongly adsorbed ($E_{ads} = -123$ kJ/mol) due to the weaker basicity of the molecule which interacts through the phenyl ring. In this hierarchy of adsorption, organosulfur compounds (DBT, alkyl-DBT) and aromatic compounds (benzene or naphtalene) are far less strongly adsorbed species on the active sites. This result clearly points out the strong inhibitor effects of basic nitrogen compounds for HDT reactions. Recent DFT investigations on the adsorption of organonitrogen compounds on NiMoS model provide similar results confirming the stronger adsorption of basic nitrogen compounds [101,102]. These results confirm the still growing potentiality of the DFT techniques to explore complex questions such as inhibitor effects playing a key role in heavy cuts.

3.2. The support as a "chemical ligand" of the active phase?

Many experimental works undertaken by Breysse et al. revealed that support effects cannot be overlooked when investigating active phase catalytic properties [31,32]. At an industrial scale, γ-alumina is the preferred support due to its well optimized textural and acidic properties [29]. At a laboratory scale, studies are still in progress to improve the properties of anatase phase of TiO_2 [103]. One well known experimental result is that the anatase-TiO_2 supported MoS_2

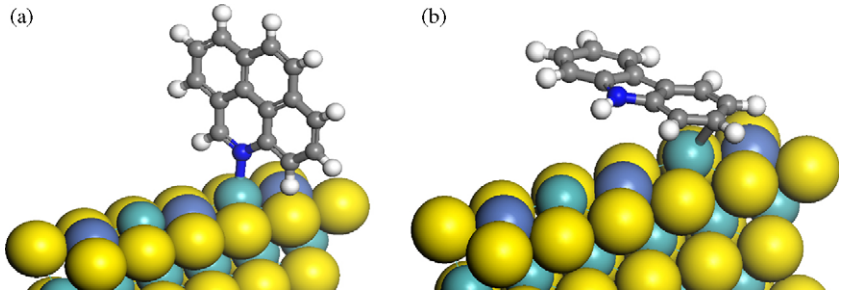

Fig. 8. Simulation of the adsorption of two relevant organonitrogen compounds on the Mo site of NiMoS catalyst: (a) benzophenantridine ($E_{ads} = -197$ kJ/mol); (b) carabazole ($E_{ads} = -123$ kJ/mol) (yellow balls: sulfur, magenta balls; molybdenum, blue balls: nickel, green balls: molybdenum, dark blue balls: nitrogen, grey balls: carbon, white balls: hydrogen). (For interpretation of the references to colour in this figure legend, the reader is referred to the web version of the article.)

catalyst exhibited a significant higher intrinsic HDS activity than γ-alumina supported MoS_2 [33]. Even if part of the synergy effect is lost on TiO_2, these observations prompted further attention devoted to the TiO_2 effect on the active phase. Understanding such a complex and subtle effect requires a detailed description of the nature of the interaction between the chemical species present at the support surface and the edge sites of the active phase. One key question for atomistic investigation is: may Mo–O–Al(Ti) or Mo–S–Al(Ti) chemical bridges connecting the two systems exist in HDS reactions? If it was the case, the active phase should not be considered as an isolated MoS_2 or Co(Ni)MoS phase but rather as a binary phase involving electronic redistribution between the oxide phase and the sulfide phase, where the support can be regarded as a ''chemical ligand'' or eventually as a ''co-catalyst'' of the active phase, using the terminology of heterogeneous catalysis. In contrast, only weak ''physical'' interactions such as van der Waals or hydrogen bonding might take place between the sulfur atoms of the basal plane of the active phase and oxygen atoms or hydroxyls of the support. In this case, the active phase should be regarded as an isolated ''raft'' on the support which acts as a dispersing agent without strong chemical influence. According to the type of interaction, the electronic properties and also the orientation of the MoS_2 sheets are modified, which may affect the reactivity of the active sites.

Very few experimental techniques are able to give direct nano-scale insights on the Co(Ni)MoS–support interface. Leliveld et al. [38] furnished an evaluation of Mo–O distances by EXAFS, assigned to MoS_2 particles interacting with the support. Using TEM, Shimada furnishes insights on the orientation of the MoS_2 sheets [34], but this technique suffers from the limitation of projecting a 3D image into 2D. Electron tomography will be of great help to better visualize and understand the orientation of supported MoS_2 sheets in the near future [104].

Concerning DFT simulations, these questions are very challenging at different levels. As for the active phases (see Section 3.1), relevant surface models of the supports in HDS conditions have to be developed. Then, models for the interacting systems have also to be investigated with great care because the size of the simulated supercell (close to 300 atoms are required in some cases) is close to the limit of current DFT techniques (even when using high performance computers). Another limiting problem is raised by the capability of the human mind to imagine – not all but at least – the relevant configurations in complex cells. At this stage, the role of modeler's chemical intuition remains crucial and any new experimental input must be considered with care to improve the models.

The few theoretical studies available in the literature for alumina supported sulfides [105–107] suffer from weaknesses in the models describing the support surfaces. To overcome these, a systematic DFT determination of γ-alumina and anatase-TiO_2 surfaces was mandatory. The lack of a precise crystallographic structure of γ-alumina has prompted DFT to bring new insights into the bulk structure of this material. Considering the topotactic transformation of boehmite (the hydrated precursor) into γ-alumina reveals the existence of non-spinel Al sites [108] also confirmed by other theoretical investigations [109,110]. The second step is the determination of the stable species in HDS conditions at the surface of γ-alumina and anatase-TiO_2 [111–114]. The thermodynamic approach explained in Section 2 is again successful in establishing surface models for various reaction conditions including HDS (p_{H_2O}, p_{H_2S}, p_{H_2} and T). The key results of these works are summarized as follows:

- The degree of hydroxylation and nature of hydroxyl species depend on the crystallographic orientation of the surface and thus on support morphologies. The anatase-TiO_2(1 0 1) and γ-alumina(1 0 0) surfaces remain non-hydroxylated in HDS conditions. The anatase-TiO_2(0 0 1) and γ-alumina(1 1 0) surfaces are hydroxylated.
- The anatase-TiO_2(0 0 1) surface is also partially sulfided, providing an explanation for the core level shift of Ti as observed by Coulier et al. [36] induced by sulfo-reductive environment (see Fig. 9). Table 1 reports the calculated surface species concentrations for TiO_2 and γ-Al_2O_3.
- The calculation of OH stretching frequencies furnishes a new assignment of the OH bands observed in the IR spectrum of anatase-TiO_2 and γ-alumina [115]. In particular, the Knözinger's assignment [26] for γ-alumina is challenged [111,112].
- Modifying the morphology may provide new ways to control the acid–base properties of the supports [113,116].

These results are thus crucial for further DFT investigations of support effects on the active phase as undertaken very recently by Arrouvel et al. [48,117]. Indeed, this work shows that these effects can only be described correctly with realistic surface models of the supports taking into account its hydroxylation or sulfidation state in reaction conditions. A

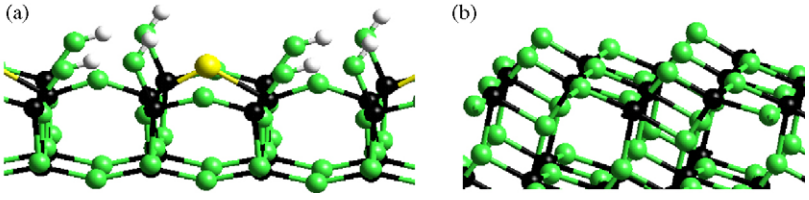

Fig. 9. (a) Hydroxylated and partially sulfided (0 0 1) surface of anatase-TiO_2 and (b) non-hydroxylated and non-sulfided (1 0 1) surface (yellow balls: sulfur, green balls: oxygen, black balls: titanium, white balls: hydrogen) (from Ref. [114]). (For interpretation of the references to colour in this figure legend, the reader is referred to the web version of the article.)

Table 1
Surface species concentrations (species/nm^2) at $p_{H_2S} = 1$ bar and $p_{H_2} = 30$ bar and for the given morphologies and different T (K). and p_{H_2O} (bar)

Support	p_{H_2O}	$T = 400$	$T = 600$
TiO_2 (1 0 1) 96%	10^{-2}	0.67 [OH]	0.14 [OH] + 0.07 [S]
TiO_2 (0 0 1) 4%	10^{-5}	0.27 [OH] + 0.14 [S]	0.14 [OH] + 0.07 [S]
γ-Al_2O_3 (1 0 0) 20%	10^{-2}	7.10 [OH]	7.10 [OH]
γ-Al_2O_3 (1 1 0) 80%	10^{-5}	7.10 [OH]	4.74 [OH]

Extracted from Ref. [114].

systematic approach based on DFT thermodynamic models of the binary phase TiO_2- and γ-Al_2O_3-supported Mo_6S_n clusters is undertaken where n varies according to the chemical potential of sulfur fixed by the HDS reaction conditions. The four above-mentioned crystallographic surfaces of γ-alumina and anatase-TiO_2 are considered. As represented in Figs. 10 and 11, the Gibbs free energy diagram of the Mo_6S_n clusters shows that for high chemical potential of sulfur (i.e. strong sulfiding conditions), the stable Mo_6S_{24} cluster is fully sulfided on both supports and is adsorbed in parallel mode: a ''raft'' like mode, such as shown in Fig. 12(a) for the (1 1 0) γ-Al_2O_3 surface. Weak van der Waals or hydrogen bonding interactions take place between the sulfur atoms of the cluster and with hydroxyls or with oxygen atoms. In a more reductive environment, Mo_6S_{14} or Mo_6S_{13} clusters are stable in a perpendicular orientation with Mo–O–Al or Mo–O(S)–Ti chemical bonds (Fig. 12(b)–(d)). The DFT optimized Mo–O lengths (about 2.0 Å) are compatible with EXAFS distances reported in the literature [38].

The most striking result is observed for anatase-TiO_2, where there is an epitaxial relationship between the Mo-edge of the Mo_6S_{14} or Mo_6S_{13} clusters and the surface oxygen and titanium atomic networks as visualized in Fig. 12(c) and (d). Even if this epitaxial relationship is not perfect due to slight mismatch between Mo–Mo and Ti–Ti distances, the local epitaxial relationship involving finite edge lengths contributes to the stabilization of strongly interacting particles with limited sizes.

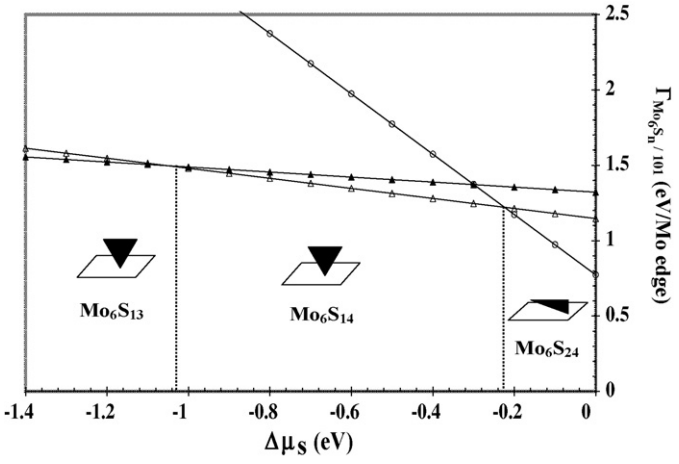

Fig. 10. Gibbs free energy diagram of the Mo_6S_n clusters adsorbed on the γ-alumina (1 1 0) surface. (○) Mo_6S_{24} (||); (△) Mo_6S_{14} (⊥); (▲) Mo_6S_{13} (⊥) (only the most stable configurations are represented, extracted from Ref. [48]).

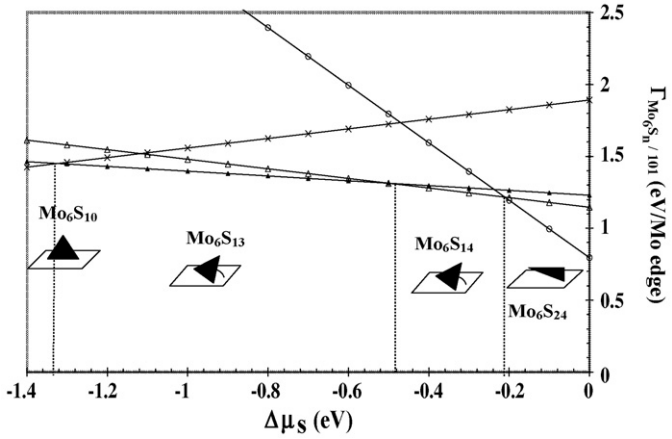

Fig. 11. Gibbs free energy diagram of the Mo_6S_n clusters adsorbed on the anatase-TiO_2 (1 0 1) surface. (○) Mo_6S_{24} (||); (△) Mo_6S_{14} (tilted); (▲) Mo_6S_{13} (tilted); (×) Mo_6S_{10} (⊥) (only the most stable configurations are represented, extracted from Ref. [48]).

This behavior not observed for γ-alumina is at the origin of the stronger ''chemical ligand effect'' of anatase-TiO_2 in HDS conditions, which induces:

- tilted orientations are stable on anatase even for larger MoS_2 crystallites (up to an edge length of about 45 Å according to Ref. [48]) which seems to be coherent with TEM observations [34];
- these strong interacting particles are chemically modified by the support: they are more sulfur deficient than ''raft'' layers, an effect which may be at the origin of the higher HDS activities observed for anatase supported MoS_2 catalysts.

In contrast, the weaker ligand effect of γ-alumina (in HDS reaction conditions) implies that only very small crystallites (for edge lengths smaller than 10 Å) develop chemical interactions with the support. In this case, the chemical ligand role of the support is reduced and this may explain the different effect of anatase-TiO_2 on the catalytic activity of non-promoted MoS_2 particles. To a certain extent, anatase-TiO_2 can be regarded as a co-catalyst of the MoS_2 phase, whereas γ-Al_2O_3 remains more passive.

Recent DFT simulations of supported CoMoS propose to explain the loss of promoting effects on anatase-TiO_2 supports observed experimentally by a different distribution of M-edge and S-edge sites induced by the epitaxial relationship [117].

3.3. Volcano curves and activity prediction of new active phases

The DFT investigations reported in the two previous sections aim at one main objective: the better understanding of industrial Co(Ni)MoS active phases to offer new concepts helping to achieve improvements in their resulting catalytic activities. Remembering the Niels Bohr's remark ''Prediction is very difficult, especially if it is about the future'', it is even more challenging and exciting for DFT simulations to assert itself as a predictive technique in order to be a rational guide for new

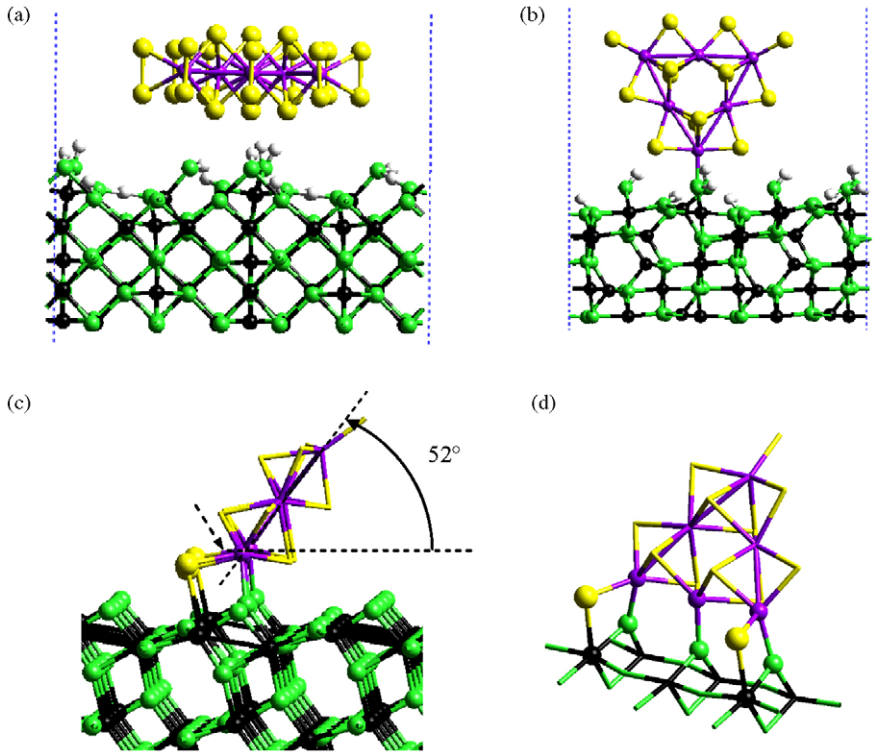

Fig. 12. Optimized structures of (a) "raft" like Mo_6S_{24} cluster on the hydroxylated (1 1 0) γ-alumina surface, (b) perpendicular Mo_6S_{14} cluster on the hydroxylated (1 1 0) γ-alumina surface, and (c) (resp. (d)) tilted Mo_6S_{14} (resp. Mo_6S_{13}) clusters on the (1 0 1) anatase-TiO_2 (with epitaxy). Yellow balls: sulfur, magenta balls: molybdenum, green balls: oxygen, white balls: hydrogen, black balls: aluminum in (a) and (b), titanium in (c) and (d) (from Ref. [48]). (For interpretation of the references to colour in this figure legend, the reader is referred to the web version of the article.)

experiments. In the context of high throughput experimentations (HTE), a recent round table of experts in the field [118] underlined that the role of molecular modeling is certainly indispensable in helping the development process for catalysis, providing chemical descriptors and establishing a robust basis for exploring new phases. Indeed, DFT calculations of relevant energy descriptors are well suited for providing a predictive approach: for instance, the binding energy of atomic nitrogen on transition metal surfaces is the relevant chemical descriptor to establish a volcano curve relationship for the catalytic activity in ammonia synthesis [119]. For HDT reactions, we have pointed out in the Section 3.1, that the sulfur–metal bond energy is a relevant intrinsic property of the active phase to be correlated with activities. More precisely, the sulfur–metal bond energy, E_{MS}, as defined in Refs. [61,94,120], correlates well with the activity via a volcano master curve (Fig. 13(a)). An analogous volcano relationship was first obtained empirically by Pecoraro and Chianelli [121] by correlating the HDS activity of DBT on bulk transition metal sulfides and the TMS experimental formation enthalpy. For a recent review on periodic trends in hydrodesulfurization catalysis the reader can refer to Ref. [122], where the different theoretical models proposed historically [123,124] are discussed in detail. One of the key result from Refs. [60,61] shows that considering the stable TMS structure in HDS conditions is crucial to get the correct electronic and energy properties. This was not the case in the earlier theoretical studies. The TMS bulk cohesive energy depends so closely on its structure that considering the wrong TMS structures leads to false the sulfur–metal bond energy values (see below).

The best agreement is obtained when the HDS activity is plotted against the DFT calculated sulfur–metal bond energy, E_{MS} defined as a partitioning of the cohesive energies among all types of bonds present in the TMS simulation cell [60,94,120]. Three relevant cases are reported in Fig. 13, corresponding to three main HDT reactions. Fig. 13(a) illustrates the volcano obtained when plotting the HDS activity as determined in the well-known work of Pecoraro and Chianelli [121] against E_{MS}. In this case, the prediction of HDS activity of mixed sulfides is also reported. The second example reported on Fig. 13(b) is for the biphenyl hydrogenation with experimental catalytic tests obtained on unsupported TMS by Lacroix et al. [125]. The third example (Fig. 13(c)) is for the toluene hydrogenation on supported TMS as obtained recently by Guernalec et al. [126,130].

These examples underline the relevance of the chemical descriptor E_{MS} in furnishing a general concept to rationalize the TMS catalytic behaviors. As explained in Section 3.1, the S–M bond energy is chemically related to the surface basicity of S species, and to the adsorption of sulfo-organic molecules, which explains qualitatively the chemical relevancy of this parameter for HDS activity. DFT investigations carried out by Aray et all. [127,128] and based on the topology of the electron density in various transition metal sulfides corroborate fully the concept's validity of sulfur–metal bond energy as defined in [61,94,120]. As Toulhoat and Raybaud proposed in

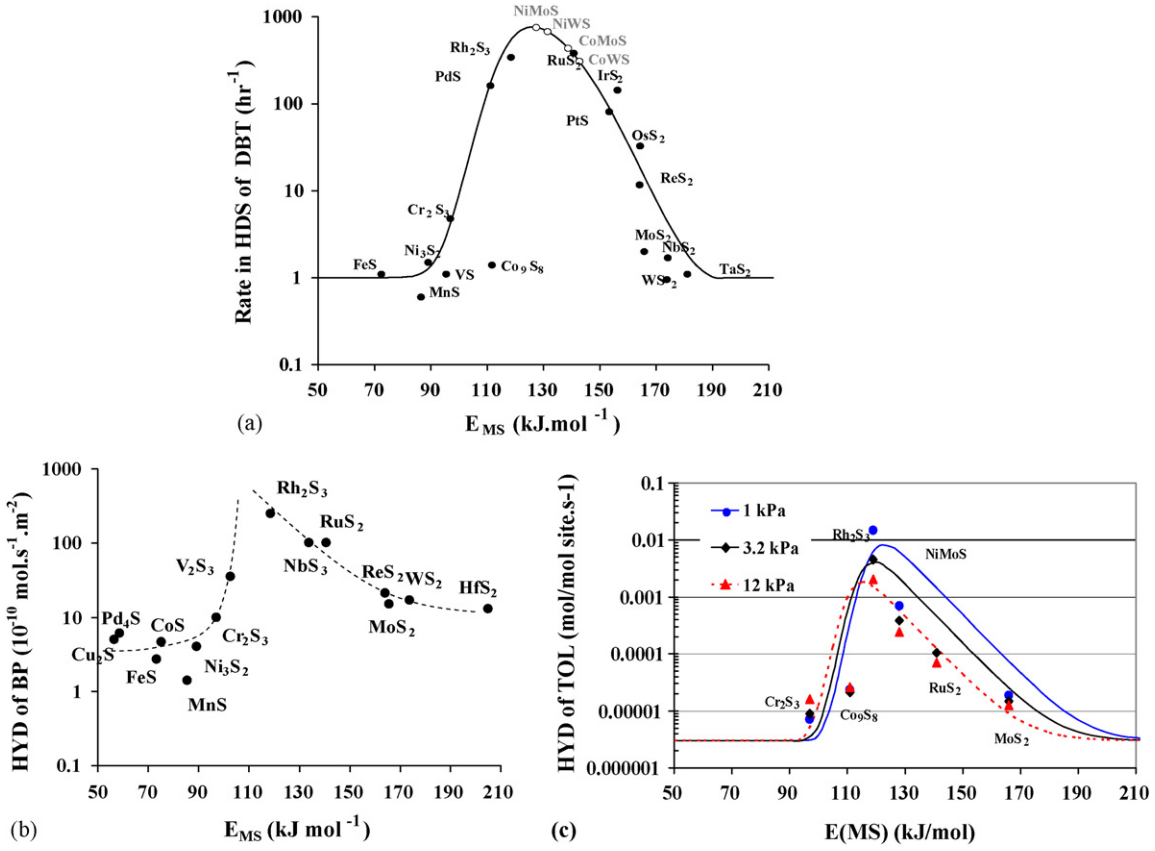

Fig. 13. Pattern of experimental activity (particle size corrected) for (a) the HDS of DBT [121] plotted against the computed E_{MS} [94]. Predictions for mixed M′Mo(W)S sulfides (○) are superimposed (“bulk” averages of E_{MS}), (b) the HYD of biphenyl [125], and (c) the HYD of toluene (from [130]) for $p(H_2S = 1, 3.2$ and 12 kPa). Lines in (a) and (c) represent the microkinetic models that best fit the data.

[60,94,120], Aray et al. recover similar volcano relationship when the HDS activity is plotted against the electronic density at the sulfur-metal bond critical point (Fig. 14), which is expected to correlate directly with the covalency of the S–M bond. In particular, 3d TMS exhibit the lowest S–M bond energies contrasting with the bond energy model proposed in Ref. [123].

A close analysis of the volcanoes reported in Fig. 13, confirms the importance of considering the stable structure in reaction conditions. According to XRD observations, stability of three TMS phases depends on the reaction conditions found in HDS of DBT [121], or in the HYD of BP [125]: VS versus V_2S_3, NbS_2 versus Nb_2S_3, and PdS versus Pd_4S sulfides. For these three TMS, the values of E_{MS} vary significantly as a function of the phase which explains their rather different BP HYD activities.

In the spirit of the Sabatier’s principle [129], an intermediate sulfur–metal bond strength corresponds to an optimal catalyst. The quantitative explanation of such volcano correlations is furnished by microkinetic modeling where the Langmuir–Hinshelwood rate expressions contain energetic values (adsorption enthalpy of reactants and relevant intermediates and activation energies) being linearly dependant on E_{MS}, i.e. a Brönsted–Evans–Polanyi type’s relationship [94,119,130]. The curves plotted in Fig. 13(a) and (c) represent the best fits of such kinetic modeling. Fig. 13(c) shows how the partial pressure of H_2S can also be included in this model. The recent result by Guernalec et al. put forwards the dual effect of H_2S on the toluene hydrogenation: for sulfide catalysts with low E_{MS} values, H_2S may enhance the catalytic activity, whereas for

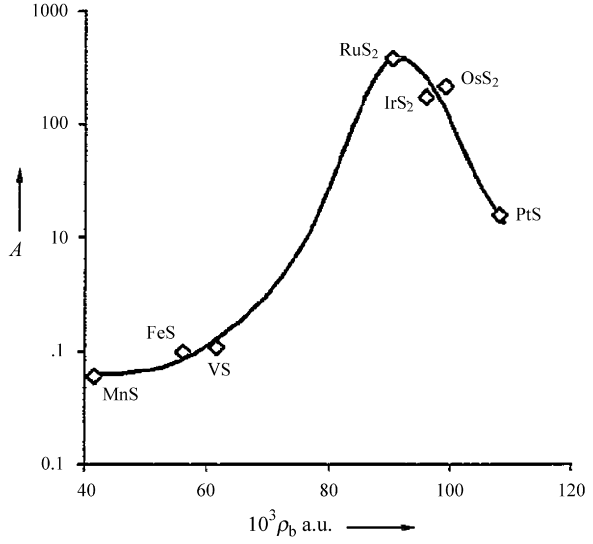

Fig. 14. HDS activity A (10^{16} molecules of DBT converted per mole and per second [121]) of the TMS as a function of the electron density at the sulfur–metal bond critical point (from Ref. [127]).

intermediate or high E_{MS} values, H_2S exhibits an inhibiting effect [130]. The microkinetic modeling also shows that the position of the optimal sulfide catalyst in the E_{MS} scale (i.e. maximum of the volcano) is displaced when changing the partial pressure of H_2S. By giving a formal determination of the surface species (free sites, reactants, intermediates, sulfhydryl groups, etc.), it is observed that the surface of catalysts with high E_{MS} values (such as MoS_2) is poisoned by S-species (as previously discussed). Intermediate E_{MS} values such as found for Co(Ni)MoS catalysts favor an optimal surface distribution of the various species involved in the reaction.

Experimental work by Bezverkhyy et al. [131] preparing highly dispersed pentladites ($M_xM'_{9-x}S_8$ type, with M = Fe, Co, Ni) sulfides exhibiting low sulfur–metal bond energies are finally all found with low thiophene HDS activity. The lowest activity is shown by $FeCo_8S_8$ phase as can be expected when considering the averaged E_{MS} value between Co_9S_8 and FeS. The predictive potentiality of such an approach can be confirmed with the example of the $NiCr_2S_4$ phase. Considering either the spinel type structure (space group *Fd*-3*m*) or the *C*2/*m* structure, the E_{MS} average value is either 111.4 or 129.4 kJ/mol which situates this phase in the windows of activity defined in Fig. 13. Other experimental work by Thiollier et al. [132] revealed that this phase is highly active in thiophene HDS and tetraline HYD. Finally, the reader can also refer to the paper by Thomazeau et al. in this volume revealing how the volcano curve concept can be applied to even more complex Co(Ni)MoWS active phases [133].

Even if the E_{MS} descriptor is an intrinsic property of bulk TMS phases, it is a good compromise for capturing the relevant intrinsic chemical properties of the TMS materials and achieving systematic DFT calculations at a large scale. To improve this approach in the future would be to include systematic studies of TMS surfaces are undertaken in order to identify surface chemical descriptors as it has been achieved for specific reactions at metal surfaces [134]. Besides Co(Ni)Mo(W)S studies presented in this review, it can be stressed that relevant DFT data already exist for RuS_2 [135,136]. This must be an interesting route to explore in a consistent way the periodic trends including more types of catalytic surfaces and morphologies in the future.

Beside microkinetic modeling, advanced theoretical approaches such as kinetic Monte Carlo, also called "*first principles* statistical mechanics" [137] may enable to determine more rigorously reaction rates and disordered species distribution in the future. To our knowledge, a first example applied to sulfides has been presented by Rusanen et al. for simulating temperature programmed reduction (TPR) spectra of MoS_2 catalyst [138]. However, this methodology not yet mature to be applied systematically to various type of sulfide surfaces requires further research works.

4. Conclusions and perspectives

This paper provides an overview of recent advances in the understanding of physico-chemical properties of transition metal sulfides achieved by *first principles* approaches. DFT simulations help to offer new highlights on some open questions of the long TMS experimental story: localization of the promoter, local structure of the Co(Ni)MoS phase, thermodynamic stability of the mixed phase in reaction conditions. DFT energy values combined with a thermodynamic model furnish the best way to make the bridge between experiment and theory. DFT combined with cutting-edge techniques (EXAFS, IR, STM) put forward rather new concepts such as morphology effects in reaction conditions. DFT also reveals for the first time the different configurations of crystallite decoration by Ni and Co. It may be that further experimentation will provide this experimental confirmation.

Regarding the investigation of the activity itself, numerous published data are now available on hydrogen activation by MoS_2 and Co(Ni)MoS phases highlighting the role of the promoter in H_2 activation. First DFT investigations of the HDS pathways of 4,6-DMDBT have been recently proposed. Further investigations in connection with the inhibiting role of nitrogen compounds are certainly required in the context of crude heavy oils.

The continuous enrichment of DFT database (energy values and atomistic configurations for numerous types of molecular compounds) of the Co(Ni)MoS active phases may simultaneously contribute to encourage emerging theoretical approaches such as kinetic Monte Carlo methods. When such methods become sufficiently mature, they will provide new ways of predicting HDS reaction rates (as measured in laboratory's catalytic tests) by combining the atomistic state of the catalytic surface and the statistical distribution of the chemical events.

As far as the role of the support is concerned, DFT simulation have recently been shown to give new insights at an atomic scale on the interface between Co(Ni)MoS and γ-alumina. This is a difficult task for any available experimental techniques, even the most advanced ones. New detailed DFT results propose relevant surface model for oxides (γ-alumina, anatase-TiO_2, etc.) useful to investigate how the interaction takes place. The concept of the ligand effects of γ-alumina and anatase-TiO_2 on the MoS_2 active phase is relevant to explain how the support has an impact on the observed catalytic activity. Emerging characterization technique such as 3D-tomography applied to sulfides may be useful to confront the DFT predictions. Furthermore, the role of the support nanoparticles morphology also enables a control of support effects. Even if this challenge is certainly tremendous (regarding the complexity of the system), the task of the simulation must be pursued if one wants to achieve in a near future the complete modeling of a supported TMS catalysts in presence of organosulfur molecules.

As another challenging perspective for DFT simulations, it is certainly requested to devote more investigations on the preparation and genesis of the active phases. For this purpose, it is required to consider the interaction of oxide active phase precursor with the γ-alumina supports. In the same spirit as achieved for the chlorinated γ-alumina surfaces [111], ionic exchanges between hydroxyl species of the support and ionic species (precursors, chelating agents, dopes, etc.) in aqueous

media at the preparation steps could be suggested for future works. Such investigations will certainly require to use hybrid methods [139] combining DFT to describe accurately the local chemical interactions and force-fields or semi-empirical parameterized Hamiltonians to include solvant effects.

In the spirit of high throughput experimentation, DFT bond energy activity descriptors such as volcano curves are very promising as a first screening tool. Examples shown in this paper reveal in which direction DFT approaches must go in order to become more predictive. Of course, the design of a new HDS catalyst by computer simulation is not for tomorrow. To bring it closer, the DFT chemical descriptor database for sulfides must be continuously improved by simulations through investigation of a greater variety of potential active phases (sulfides, nitrides, carbides, etc.) and supports.

First principles modeling asserted itself as a versatile tool to investigate complex issues raised by HDT catalysis. It may go beyond the point of which traditional techniques are reaching their limits, and it furnishes new guides and concepts for experimentalists, while keeping a vivid place for intuition. For sure, it is now an integral part of the research activity on catalytically active phases in hydrotreatment.

Acknowledgements

Part of the works referenced herein have been undertaken within the Groupement de Recherche Européen ''Dynamique Moléculaire Quantique Appliquée à la Catalyse'', a joint project of IFP-CNRS-TOTAL-Universität Wien. P. Raybaud addresses a special thank to Michèle Breysse for her very fruitful collaboration and for having shared her experience in the field. P. Raybaud is also grateful to IFP's colleagues, particularly to H. Toulhoat and M. Digne, and to J. Hafner, G. Kresse from Universität Wien (Austria), P. Sautet from Ecole Normale Supérieure de Lyon (France), and to D. Costa from UPMC, C. Arrouvel, H. Schweiger, G. Izzet for their contribution to numerous works.

References

[1] J.C. Plumail, Proceedings of the ARTC Seventh Annual Meeting Incorporating the ARTC, Singapore, 2004 (http://www.axens.fr/html-gb/events/conference-representation.html).
[2] E. Benazzi, C. Cameron, in: HART (Eds.), World Diesel Clean Technology, World Diesel Report, 2005, pp. 6–11.
[3] H. Topsøe, B.S. Clausen, F.E. Massoth, in: J.R. Anderson, M. Boudart (Eds.), Hydrotreating Catalysis—Science and Technology, 11, Springer-Verlag, Berlin, 1996.
[4] R. Prins, in: G. Ertl, H. Knözinger, J. Weitkamp (Eds.), Handbook of Heterogeneous Catalysis, 4, Wiley/VHC Verlagsgesellschaft, Weinheim, 1997, p. 1908.
[5] F. Delannay, Appl. Catal. 16 (1985) 135.
[6] E. Payen, S. Kasztelan, S. Houssenbay, R. Szymansky, J. Grimblot, J. Phys. Chem. 93 (1989) 6501.
[7] I. Alstrup, I. Chorkendorff, R. Candia, B.S. Clausen, H. Topsoe, J. Catal. 77 (1982) 397.
[8] S. Kasztelan, J. Grimblot, J.P. Bonnelle, E. Payen, H. Toulhoat, Y. Jacquin, Appl. Catal. 7 (1983) 91.
[9] F.B. Garreau, H. Toulhoat, S. Kasztelan, R. Paulus, Polyhedron 5 (1986) 211.
[10] S. Houssenbay, S. Kasztelan, H. Toulhoat, J.P. Bonnelle, J. Grimblot, J. Phys. Chem. 93 (1989) 7176.
[11] C. Wivel, R. Candia, B.S. Clausen, S. Mørup, H. Topsøe, J. Catal. 68 (1981) 453.
[12] E. Payen, S. Kasztelan, J. Grimblot, J. Mol. Struct. 174 (1988) 71.
[13] B.S. Clausen, H. Topsøe, R. Candia, J. Villadsen, B. Lengeler, J. Als-Nielsen, F. Christensen, J. Phys. Chem. 85 (1981) 3868.
[14] B.S. Clausen, H. Topsøe, Hyperfine Interact. 47 (1989) 203.
[15] S.M.A.M. Bouwens, D.C. Koningsberger, V.H.J. de Beer, S.P.A. Louwers, R. Prins, Catal. Lett. 5 (1990) 273.
[16] C. Calais, N. Matsubayashi, C. Geantet, Y. Yoshimura, H. Shimada, A. Nishijima, M. Lacroix, M. Breysse, J. Catal. 174 (1998) 130.
[17] T. Shido, R. Prins, J. Phys. Chem. 102 (1998) 8426.
[18] N.-Y. Topsøe, H. Topsøe, J. Catal. 84 (1983) 386.
[19] F. Maugé, J.C. Duchet, J.C. Lavalley, S. Houssenbay, E. Payen, J. Grimblot, S. Kasztelan, Catal. Today 10 (1991) 561.
[20] M.P. De la Rosa, S. Texier, G. Berhault, A. Camacho, M.J. Yacaman, A. Mehta, S. Fuentes, J.A. Montoya, F. Murrieta, R.R. Chianelli, J. Catal. 225 (2004) 288.
[21] B.C. Lippens, J.H. de Boer, Acta Crystallogr. 17 (1964) 1312.
[22] J. Hietala, A. Root, P. Knuuttila, J. Catal. 150 (1994) 46.
[23] E.C. De Canio, J.C. Edwards, J.W. Bruno, J. Catal. 148 (1994) 76.
[24] D. Guillaume, S. Gautier, F. Alario, J.M. Devès, Oil Gas Sci. Technol. Rev. IFP 54 (4) (1997) 537.
[25] A.A. Tsyganenko, V.N. Filimonov, J. Mol. Struct. 19 (1973) 579.
[26] H. Knözinger, P. Ratnasamy, Catal. Rev. Sci. Eng. 17 (1978) 31.
[27] C. Morterra, G. Magnacca, Catal. Today 27 (1996) 497.
[28] A.B. Mohammed Saad, V.A. Ivano, J.C. Lavalley, P. Nortier, F. Luck, Appl. Catal. 94 (1993) 71.
[29] P. Euzen, P. Raybaud, X. Krokidis, H. Toulhoat, J.-L. Le Loarer, J.-P. Jolivet, C. Froidefond, in: F. Schüth, K.S.W. Sing, J. Weitkamp (Eds.), Handbook of Porous Solids, vol. 3, Wiley/VCH Verlag GmbH, Weinheim, 2002, p. 1591.
[30] P. Nortier, P. Fourre, A.B. Mohammed Saad, O. Saur, J.-C. Lavalley, Appl. Catal. 61 (1990) 141.
[31] M. Breysse, J.L. Portefaix, M. Vrinat, Catal. Today 10 (1991) 489.
[32] M. Breysse, P. Afanasiev, C. Geantet, M. Vrinat, Catal. Today 86 (2003) 5.
[33] J. Ramirez, S. Fuentes, G. Díaz, M. Vrinat, M. Breysse, M. Lacroix, Appl. Catal. 52 (1989) 211.
[34] H. Shimada, Catal. Today 86 (2003) 17.
[35] J. Ramirez, L. Cedeno, G. Busca, J. Catal. 184 (1999) 59.
[36] L. Coulier, J.A.R. van Veen, J.W. Niemantsverdriet, Catal. Lett. 79 (2002) 149.
[37] D. Wang, W. Qian, A. Ishihara, T. Kabe, Appl. Catal. A: Gen. 224 (2002) 191.
[38] R.G. Leliveld, A.J. van Dillen, J.W. Geus, D.C. Koningsberger, J. Catal. 165 (1997) 184.
[39] P. Hohenberg, W. Kohn, Phys. Rev. B 136 (1964) 864.
[40] W. Kohn, L.J. Sham, Phys. Rev. A 140 (1965) 1133.
[41] G. Kresse, J. Furthmüller, Comput. Mater. Sci. 6 (1996) 15.
[42] http://cms.mpi.univie.ac.at/vasp.
[43] http://www.camp.dtu.dk/campos.
[44] http://www.wien2k.at.
[45] M.C. Payne, M.P. Teter, D.C. Allan, T.A. Arias, J.D. Joannopoulos, Rev. Mod. Phys. 64 (1992) 1045.
[46] $DMol^3$ and CASTEP are commercialised within the Materials Studio graphical user interface by Accelrys: http://www.accelrys.com.
[47] B. Delley, J. Chem. Phys. 113 (2000) 7756.
[48] C. Arrouvel, M. Breysse, H. Toulhoat, P. Raybaud, J. Catal. 232 (2005) 161.
[49] G.X. Quian, R.M. Martin, D.J. Chadi, Phys. Rev. B 38 (11) (1988) 7649.
[50] K. Kadas, G. Kern, J. Hafner, Phys. Rev. B 58 (23) (1998) 1.
[51] X.-G. Wang, W. Weiss, Sh.K. Shaikhutdinov, M. Ritter, M. Petersen, F. Wagner, R. Schlögl, M. Scheffler, Phys. Rev. Lett. 81 (1999) 1038.
[52] P. Raybaud, J. Hafner, G. Kresse, S. Kasztelan, H. Toulhoat, J. Catal. 189 (2000) 129.

[53] P. Raybaud, J. Hafner, G. Kresse, S. Kasztelan, H. Toulhoat, J. Catal. 190 (2000) 128.
[54] S. Cristol, J.-F. Paul, E. Payen, D. Bougeard, S. Clémendot, F. Hutschka, J. Phys. Chem. B 104 (2000) 11220.
[55] M.V. Bollinger, K.W. Jacobsen, J.K. Nørskov, Phys. Rev. B 67 (2003) 085410.
[56] J.P. Perdew, Y. Wang, Phys. Rev. B 45 (1992) 13244.
[57] D. Vanderbilt, Phys. Rev. B 41 (1990) 7892.
[58] G. Kresse, J. Hafner, Phys. Rev. B 49 (1994) 14251.
[59] G. Kresse, D. Joubert, Phys. Rev. B 59 (1999) 1758.
[60] P. Raybaud, J. Hafner, G. Kresse, H. Toulhoat, J. Phys. Condens. Matter. 9 (1997) 11107.
[61] P. Raybaud, J. Hafner, G. Kresse, H. Toulhoat, J. Phys. Condens. Matter 9 (1997) 11085.
[62] D. Hobbs, J. Hafner, J. Phys. Condens. Matter 11 (1999) 8197.
[63] A. Rohrbach, J. Hafner, G. Kresse, J. Phys. Condens. Matter 15 (2003) 979.
[64] G. Mills, H. Jonsson, G.K. Schenter, Surf. Sci. 324 (1995) 305.
[65] J. Hafner, L. Benco, T. Bucko, Top. Catal. 37 (2006) 41.
[66] D. Loffreda, F. Delbecq, F. Vigne, P. Sautet, J. Am. Chem. Soc. 128 (2006) 1316.
[67] P. Raybaud, J. Hafner, G. Kresse, H. Toulhoat, Surf. Sci. 407 (1998) 237.
[68] T. Todorova, V. Alexiev, R. Prins, T. Weber, Phys. Chem. Chem. Phys. 6 (2004) 3023.
[69] A. Travert, C. Dujardin, F. Mauge, S. Cristol, J.F. Paul, E. Payen, D. Bougeard, Catal. Today 70 (2001) 255.
[70] L.S. Byskov, J.K. Nørskov, B.S. Clausen, H. Topsøe, J. Catal. 187 (1999) 109.
[71] P. Raybaud, J. Hafner, G. Kresse, H. Toulhoat, Phys. Rev. Lett. 80 (1998) 1481.
[72] H. Schweiger, P. Raybaud, G. Kresse, H. Toulhoat, J. Catal. 207 (2002) 76.
[73] S. Helveg, J.V. Lauritsen, E. Lægsgaard, I. Stensgaard, J.K. Nørskov, B.S. Clausen, H. Topsøe, F. Besenbacher, Phys. Rev. Lett. 84 (2000) 951.
[74] J.V. Lauritsen, M.V. Bollinger, E. Lægsgaard, K.W. Jacobsen, J.K. Nørskov, B.S. Clausen, H. Topsøe, F. Besenbacher, J. Catal. 221 (2004) 510.
[75] S. Cristol, J.-F. Paul, E. Payen, D. Bougeard, S. Clémendot, F. Hutschka, J. Phys. Chem. B 106 (2002) 5659.
[76] J.-F. Paul, E. Payen, J. Phys. Chem. B 107 (2003) 4057.
[77] A. Travert, H. Nakamura, R.A. van Santen, S. Cristol, J.F. Paul, E. Payen, J. Am. Chem. Soc. 124 (2002) 7084.
[78] M.Y. Sun, A.E. Nelson, J. Adjaye, J. Catal. 233 (2005) 411.
[79] P. Raybaud, J. Hafner, G. Kresse, H. Toulhoat, Stud. Surf. Sci. Catal. (Hydrotreatment and Hydrocracking of Oil Fractions) 127 (1999) 309.
[80] S. Cristol, J.F. Paul, E. Payen, D. Bougeard, J. Hafner, F. Hutschka, Stud. Surf. Sci. Catal. (Hydrotreatment and Hydrocracking of Oil Fractions) 127 (1999) 327.
[81] S. Cristol, J.F. Paul, E. Payen, D. Bougeard, F. Hutschka, S. Clemendot, J. Catal. 224 (2004) 138.
[82] J.V. Lauritsen, M. Nyberg, J.K. Nørskov, B.S. Clausen, H. Topsøe, E. Lægsgaard, F. Besenbacher, J. Catal. 224 (2004) 94.
[83] J.V. Lauritsen, M. Nyberg, R.T. Vang, M.V. Bollinger, B.S. Clausen, H. Topsoe, K.W. Jacobsen, E. Laegsgaard, J.K. Norskov, F. Besenbacher, Nanotechnology 14 (2003) 385.
[84] R.J.H. Voorhoeve, J.C.M. Stuiver, J. Catal. 23 (1971) 228.
[85] H. Schweiger, P. Raybaud, H. Toulhoat, J. Catal. 212 (2002) 33.
[86] J.V. Lauritsen, S. Helveg, E. Lægsgaard, I. Stensgaard, B.S. Clausen, H. Topsøe, F. Besenbacher, J. Catal. 197 (2001) 1.
[87] M. Breysse, R. Frety, B. Benaïchouba, P. Bussière, Radiochem. Radioanal. Lett. 59 (1983) 265.
[88] M. Breysse, R. Frety, M. Vrinat, Appl. Catal. 12 (1984) 165.
[89] M. Sun, A.E. Nelson, J. Adjaye, J. Catal. 226 (2004) 32.
[90] M. Bremaud, L. Vivier, G. Perot, V. Harle, C. Bouchy, Appl. Catal. A: Gen. 289 (2005) 44.
[91] M. Egorova, R. Prins, J. Catal. 241 (2006) 162.
[92] A. Travert, C. Dujardin, F. Maugé, E. Veilly, S. Cristol, J.-F. Paul, E. Payen, J. Phys. Chem. B 110 (2006) 1261–1270.
[93] H. Orita, K. Uchida, N. Itoh, Appl. Catal. A: Gen. 258 (2004) 115.
[94] H. Toulhoat, P. Raybaud, J. Catal. 216 (2003) 63.
[95] M.Y. Sun, A.E. Nelson, J. Adjaye, Catal. Today 105 (2005) 36.
[96] G. Berhault, M. Lacroix, M. Breysse, F. Maugé, J.C. Lavalley, H. Nie, L.L. Qu, J. Catal. 178 (1998) 555.
[97] T. Todorova, R. Prins, T. Weber, J. Catal. 236 (2005) 190.
[98] E. Veilly, Thesis, Université de Lille, 2004.
[99] E. Veilly, J.F. Paul, S. Cristol, E. Payen, D. Bougeard, R. Le Gall, F. Hutschka, in: Proceedings of the 13th International Congress on Catalysis, Paris, 2004.
[100] F. Bataille, J.L. Lemberton, P. Michaud, G. Perot, M. Vrinat, M. Lemaire, E. Schulz, M. Breysse, S. Kasztelan, J. Catal. 191 (2000) 409.
[101] M.Y. Sun, A.E. Nelson, J. Adjaye, Catal. Today 109 (2005) 49.
[102] M.Y. Sun, A.E. Nelson, J. Adjaye, J. Catal. 231 (2005) 223.
[103] S. Dzwigaj, C. Louis, M. Breysse, M. Cattenot, V. Bellière, C. Geantet, M. Vrinat, P. Blanchard, E. Payen, S. Inoue, H. Kudo, Y. Yoshimura, Appl. Catal. B: Environ. 41 (2003) 181.
[104] U. Ziese, A.J. Koster, A.J. Verkleij, A.H. Janssen, K.P. de Jong, J. Phys. Chem. B 104 (2000) 9368.
[105] P. Faye, E. Payen, A. Datta, J. Catal. 179 (1998) 560.
[106] A. Ionescu, A. Allouche, J.-P. Aycard, M. Rajzmann, R. Le Gall, J. Phys. Chem. B 107 (2003) 8490.
[107] B. Hinnemann, J.K. Norskov, H. Topsøe, J. Phys. Chem. B 109 (2005) 2245.
[108] X. Krokidis, P. Raybaud, A.-E. Gobichon, B. Rebours, P. Euzen, H. Toulhoat, J. Phys. Chem. B 105 (2001) 5121.
[109] C. Wolverton, K.C. Haas, Phys. Rev. B 63 (2001) 024102.
[110] G. Paglia, A.L. Rohl, C.E. Buckley, J.D. Gale, Phys. Rev. B 71 (2005) 224115.
[111] M. Digne, P. Sautet, P. Raybaud, P. Euzen, H. Toulhoat, J. Catal. 211 (2002) 1.
[112] M. Digne, P. Sautet, P. Raybaud, P. Euzen, H. Toulhoat, J. Catal. 226 (2004) 54.
[113] C. Arrouvel, M. Digne, M. Breysse, H. Toulhoat, P. Raybaud, J. Catal. 222 (2004) 152.
[114] C. Arrouvel, H. Toulhoat, M. Breysse, P. Raybaud, J. Catal. 226 (2004) 260.
[115] A. Travert, O.V. Manoilova, A.A. Tsyganenko, F. Maugé, J.C. Lavalley, J. Phys. Chem. B 106 (2002) 1350.
[116] S. Dzwigaj, C. Arrouvel, M. Breysse, C. Geantet, S. Inoue, H. Toulhoat, P. Raybaud, J. Catal. 236 (2005) 245.
[117] D. Costa, C. Arrouvel, M. Breysse, H. Toulhoat, P. Raybaud, J. Catal. 246 (2007) 325.
[118] P. Raybaud, H. Toulhoat, S. Morin, D. Farrusseng, J. Norskov, G. Baron, C. Wolverton, R.R. Chianelli, Oil Gas Sci. Technol. 61 (2006) 579.
[119] A. Logadottir, T.H. Rod, J.K. Norskov, B. Hammer, S. Dahl, C.J.H. Jacobsen, J. Catal. 197 (2001) 229.
[120] H. Toulhoat, P. Raybaud, S. Kasztelan, G. Kresse, J. Hafner, Catal. Today 50 (1999) 629.
[121] T.A. Pecoraro, R.R. Chianelli, J. Catal. 67 (1981) 430.
[122] R.R. Chianelli, G. Berhault, P. Raybaud, S. Kasztelan, J. Hafner, H. Toulhoat, Appl. Catal. A: Gen. 227 (2002) 83.
[123] J.K. Nørskov, B.S. Clausen, H. Topsøe, Catal. Lett. 13 (1992) 1.
[124] S. Harris, R.R. Chianelli, J. Catal. 98 (1986) 17.
[125] M. Lacroix, N. Boutarfa, C. Guillard, M. Vrinat, M. Breysse, J. Catal. 120 (1989) 473.
[126] N. Guernalec, T. Cseri, P. Raybaud, C. Geantet, M. Vrinat, Catal. Today 98 (2004) 61.
[127] Y. Aray, J. Rodriguez, D. Vega, E.N. Rodriguez-Arias, Angew. Chem. Intern. Ed. 39 (2000) 3810.
[128] Y. Aray, J. Rodriguez, Chem. Phys. Chem. 2 (2001) 599.
[129] P. Sabatier, Berichte der Deutschen Chem. Gesellschaft 44 (1911) 2001.
[130] N. Guernalec, C. Geantet, P. Raybaud, T. Cseri, M. Aouine, M. Vrinat, Oil Gas Sci. Technol. 61 (2006) 515.

[131] I. Bezverkhyy, P. Afanasiev, M. Danot, J. Phys. Chem. B 108 (2004) 7709.
[132] A. Thiollier, P. Afanasiev, P. Delichere, M. Vrinat, J. Catal. 197 (2001) 58.
[133] C. Thomazeau, C. Geantet, M. Lacroix, M. Danot, V. Harlé, P. Raybaud, Appl. Catal. A: Gen. 322 (2007) 92.
[134] T. Bligaard, J.K. Norskov, S. Dahl, J. Matthiesen, C.H. Christensen, J. Sehested, J. Catal. 224 (2004) 206.
[135] M.E. Grillo, V. Smelyanski, P. Sautet, J. Hafner, Surf. Sci. 439 (1999) 163–172.
[136] M.E. Grillo, P. Sautet, Surf. Sci. 457 (2000) 285–293.
[137] K. Reuter, C. Stampfl, M. Scheffler, in: S. Yip (Ed.), Handbook of Materials Modeling—Ab initio Thermodynamics and Statistical Mechanics of Surface Properties and Functions, vol. 1, Springer-Verlag, Berlin, 2005.
[138] M. Rusanen, H. Toulhoat, P. Raybaud, S. Kaszetelan, P. Kratzer, in: Proceedings of the ‘‘Catalysis from First Principles’’ Conference, Magleas, Danemark, June 7–9, 2004.
[139] M. Sierka, J. Sauer, J. Chem. Phys. 112 (2000) 6983.
[140] S. Kasztelan, H. Toulhoat, J. Grimblot, J.P. Bonnelle, Appl. Cat. 13 (1984) 127.